Contents

List of Figures

List of Tables

Chapter 1

Squeezing angle fluctuations

1.1 Phase Noise due to RF sidebands

At the output port of the interferometer, the interferometer sidebands add amplitude noise to the interferometer carrier. However, the contrast defect light is out of phase with the interferometer carrier, and so the RF sidebands beating against the contrast defect light add phase noise to the light at the DC readout PDs. Imbalance of the two RF sidebands will also add phase noise to the interferometer carrier light.

1.1.1 Contrast Defect

The interferometer sidebands add amplitude noise, not phase noise to the carrier at the interferometer output. However, the contrast defect light is 90 degrees out of phase with the carrier, and so the RF sidebands create phase noise on the contrast defect. The phase noise on the contrast defect in turn adds phase noise to the carrier. From the left side of **??** we see that $\theta_1 \approx A_{cd}/A_{carr}$ and that $\theta_1 \approx x/A_{SB}$. The maximum phase excursion is

$$\delta\theta_1 \approx x/A_{carr} = \frac{A_{SB}A_{cd}}{A_{carr}^2} \tag{1.1}$$

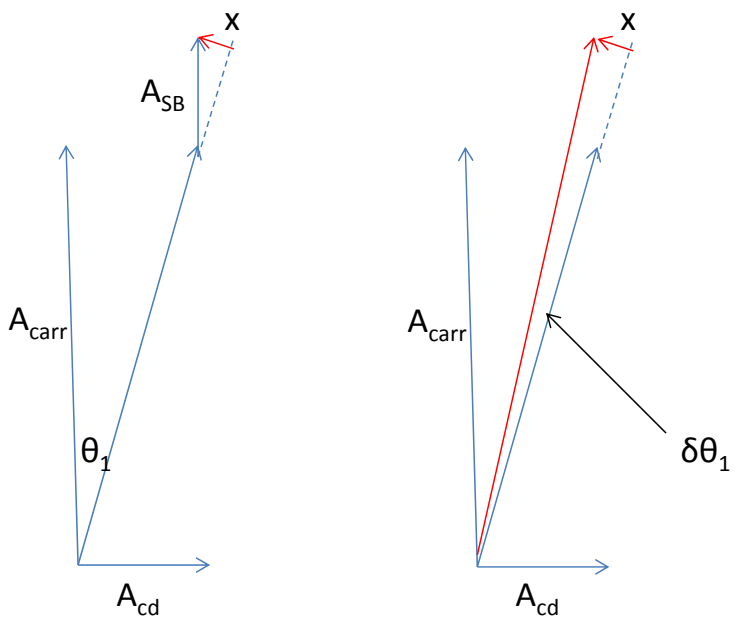

Figure 1-1: Illustration of RF sidebands and contrast defect adding phase noise to the carrier, not to scale. A_{cd} is the amplitude of the contrast defect light, A_{carr} is the amplitude of the carrier, A_{SB} is the amplitude of both the sidebands transmitted through the OMC.

The powers in each sideband $P_{SB}$is measured before the OMC, which has a power transmission of T_{SB} for the sidebands. The rms phase noise added is

$$\tilde{\theta}_{CD} = \sqrt{\frac{2T_{SB}P_{SB}P_{CD}}{P_{carr}^2}} \tag{1.2}$$

The transmission through the OMC of the RF side bands (24.5MHz offset) is

$$T_{SB} = \left| \frac{t_{in}t_{out}}{1 - \rho r_{in} r_{out} e^{\frac{2\pi f_{SB}}{f_{FSR}}}} \right|^2 = 2.35 \times 10^{-4} \tag{1.3}$$

t_{in}	input coupler amplitude transmittance	$\sqrt{8368 \times 10^{-6}}$ [?]
t_{out}	output coupler amplitude transmittance	$\sqrt{8297 \times 10^{-6}}$
r_{in}	output coupler amplitude reflectance	$\sqrt{1 - t_{in}^2}$
r_{out}	output coupler amplitude reflectance	$\sqrt{1 - t_{out}^2}$
F	Finesse	360 ± 5
ρ	other cavity losses (reflectance)	0.9996
f_{SB}	sideband frequency	24.5 MHz
f_{FSR}	free spectral range	278.3 MHz

These numbers are from T080144.

Table is not working right ! The sideband to carrier power ratio with 3.2pm DARM offset and 8W input power was 2.19 for each sideband. [?] The contrast defect power at 20W is 0.4% of the carrier power. [?] This gives 3.0±0.2 mrad of phase noise due to the RF sidebands and contrast defect.

1.1.2 Sideband Imbalance

The phase noise due to sideband imbalance is

$$\tilde{\theta} = \frac{(\sqrt{P_2} - \sqrt{P_1})\sqrt{T_{SB}}}{\sqrt{8P_{CR}}} \approx \sqrt{\frac{T_{SB} dP_{SB}^2}{8 P_{CR} \bar{P}}} \tag{1.4}$$

where $P_{2,1}$ are the powers in the 2 sidebands, $dP = P_2 - P_1$ and $\bar{P} = (P_2 + P_1)/2$. This give 0.96 ± 0.3 mrad rms phase noise due to sideband imbalance. The phase noise due t imbalance and that due to contrast defect add in quadrature to give a total of 2.8mrad phase noise from the RF sidebands, an insignificant contribution to our total phase noise.

1.1.3 SHG sidebands

The SHG has $147 \pm 1mW$ green out for $281 \pm 1mW$ in.

$$\rho = \sqrt{\frac{147 \pm 1}{281} * R1 * R2R1} \quad = 0.90 \tag{1.5}$$

$$\begin{aligned} R2 &= 0.9985 \\ f_{SB} &= 35.5MHz \\ f_{FSR} &= 3.25GHz \\ \left|\frac{E_{circ}}{E_{incident}}\right|_{35.5MHz}|^2 &= 0.98 \pm 0.01 \\ \left|\frac{E_{circ}}{E_{incident}}\right|_{carrier}|^2 &= 1.01 \pm 0.02 \\ drivetoSHGsidebandEOM &= 11.4dBm \\ radianspervoltat1064from4004EOM &= 15 \pm 2mrad \\ modulationdepthoninputbeam &= 12.5 \pm 1.5mrad \\ rmsphasenoiseat35MHzongreenbeamoutofSHG &= 11.5 \pm 1.5mrad \end{aligned} \tag{1.6}$$

RF drive to EOM for OPO is 4.83dBm (tomoki, sqwiki, documentation, reference values)

1.2 Misalignment and beam jitter

Relative misalignments between the squeezed beam and the interferometer beam change the error point of the sensor that locks the squeezing angle to the interferometer phase. This means that the squeezing angle needs to be retuned after changes in the static alignment, that static misalignments will lead to an increase in phsae noise and that even in the absence of any static misalignments jitter of the two beams will add phase noise and limit the amount of squeezing observed.

1.3 Error signal calculation with misalignments

The LO error signal is generated by the beat between the IFO field and the CLF field, both of which can have misalignments. Assuming that both fields are mostly in the 00 mode with a small component in the 10 mode at the photo detector we can write the total field at the photodetector as

$$\begin{aligned} E(x,y,z,t) &= E^{ifo} + E^{+} + E^{-} \\ &= \{(a_{00}^{ifo} u_{00}(x,y,z) + a_{ij}^{ifo} u_{ij}(x,y,z))e^{i\phi_{ifo}} \\ &+(a_{00}^{+} u_{00}(x,y,z) + a_{ij}^{+} u_{ij}(x,y,z))e^{i(\omega t+\phi_{+})} \\ &+(a_{00}^{-} u_{00}(x,y,z) + a_{ij}^{-} u_{ij}(x,y,z))e^{i(-\omega t+\phi_{-})}\}e^{i\Omega t} + c.c. \end{aligned} \tag{1.7}$$

The photocurrent will be

$$I_{PD} \propto \int_{-\infty}^{\infty} |E(x,y,z_{PD},t)|^2 dxdy \tag{1.8}$$

We can ignore terms that include products of u_{00} and u_{10} since

$$\int_{-\infty}^{\infty} u_{ij}(x,y)u_{kl}(x,y)dxdy = \delta_{ik}\delta_{jl} \tag{1.9}$$

Since this photocurrent will be demodulated at ω we can also ignore dc terms and terms at 2ω. Terms that remain are

$$I_{PD} \propto \{a_{00}^{ifo} a_{00}^{+*} e^{i(\phi_{ifo}-\phi_{+})} + a_{00}^{ifo*} a_{00}^{-} e^{i(\phi_{-}-\phi_{ifo})} + a_{ij}^{ifo} a_{ij}^{+*} e^{i(\phi_{ifo}-\phi_{+})} + a_{ij}^{ifo*} a_{ij}^{-} e^{i(\phi_{-}-\phi_{ifo})}\}e^{-i\omega t} + c.c. \tag{1.10}$$

We can assume that the u_{10} components are small compared to the u_{ij} components, and

write

$$\gamma_{ij}^{ifo} = \left| \frac{a_{ij}^{ifo}}{a_{00}^{ifo}} \right| \tag{1.11}$$
$$\gamma_{ij}^{clf} = \left| \frac{a_{ij}^{+}}{a_{00}^{+}} \right| = \left| \frac{a_{ij}^{-}}{a_{00}^{-}} \right|$$

We can also write the relative phase between the ij modes and the 00 modes as ϕ_{ij}.

$$a_{ij}^{ifo} = \gamma_{ij}^{ifo} a_{00}^{ifo} e^{i\phi_{ij}^{ifo}} \tag{1.12}$$
$$a_{ij}^{clf} = \gamma_{ij}^{clf} a_{00}^{clf} e^{i\phi_{ij}^{clf}} \tag{1.13}$$
$$\phi_{ij} = \phi_{ij}^{ifo} - \phi_{ij}^{clf} \tag{1.14}$$
$$0 = \phi_{00}^{ifo} = \phi_{00}^{clf} = \phi_{00} \tag{1.15}$$

This phase will only be nonzero when there is a misalignment that is not common to the two beams. The ratio of the amplitudes of the two coherent locking fields is

$$\alpha = \left| \frac{a_{00}^{-}}{a_{00}^{+}} \right| = \left| \frac{a_{ij}^{-}}{a_{ij}^{+}} \right| \tag{1.16}$$

Now the photocurrent can be written

$$I_{PD} \propto \cos(\phi_{ifo} - \phi_{+} - \omega t) + \alpha \cos(\phi_{-} - \phi_{ifo} - \omega t)$$
$$+\Sigma_{ij} \gamma_{ij}^{ifo} \gamma_{ij}^{clf} \left(\cos(\phi_{ifo} - \phi_{+} - \omega t + \phi_{ij}) + \alpha \cos(\phi_{-} - \phi_{ifo} - \omega t - \phi_{ij}) \right) \tag{1.17}$$

The coherent locking loop controls the phase between these two fields, $\psi \equiv \phi_{+} - \phi_{-}$. We will also write $\phi \equiv \phi_{+} - \phi_{ifo}$. The photo-current can now be written

$$I_{PD} \propto [\cos(-\phi - \omega t) + \alpha \cos(\phi - \psi - \omega t) + \Sigma_{ij} \gamma_{ij}^{ifo} \gamma_{ij}^{clf} (\cos(-\phi + \phi_{ij} - \omega t) - \alpha \cos(-\omega t - \phi + \psi + \phi_{ij})) \tag{1.}$$

This photocurrent is demodulated by signals $\cos(\omega t + \theta_{dm})$(for the I phase) and $\sin(\omega t + \theta_{dm})$ (for the Q phase), and low passed to get rid of the 2ω terms.

$$I_{err} \propto \cos(-\phi + \theta_{dm}) + \alpha \cos(\phi - \psi + \theta_{dm}) + \Sigma_{ij} \gamma_{ij}^{ifo} \gamma_{ij}^{clf} [\cos(-\phi + \phi_{ij} + \theta_{dm}) + \alpha \cos(\phi - \psi - \phi_{ij} + \theta_{dm}) \quad (1$$

$$Q_{err} \propto \sin(-\phi + \theta_{dm}) + \alpha \sin(\phi - \psi + \theta_{dm}) + \Sigma_{ij} \gamma_{ij}^{ifo} \gamma_{ij}^{clf} [\sin(-\phi + \phi_{ij} + \theta_{dm}) + \alpha \sin(\phi - \psi - \phi_{ij} + \theta_{dm}) \quad (1$$

(1

1.3.1 Error signals without misalignments

The misalignment terms will be small compared to the error signal due to the U_{00}modes, so they are a small perturbation around the locking point without any misalignments. Without any misalignments the demodulated signals are simply

$$I_{err} \propto \cos(\phi - \theta_{dm}) + \alpha \cos(\phi - \psi + \theta_{dm}) \quad (1.22)$$

$$Q_{err} \propto \sin(\theta_{dm} - \phi) + \alpha \sin(\phi - \psi + \theta_{dm}) \quad (1.23)$$

If there were no generated sideband (lower sideband in this example) the error signal would simply be a beat note, and would map out a circle in I and Q as ϕ changes. In the other extreme, where the two sidebands have equal amplitudes($\alpha = 1$) the error signal becomes a Pound Drever Hall error signal and with particular choices of the demodulation phase the signal can be zeroed in either quadrature. Our LO error signal is an intermediate case where $\alpha \approx 0.23$(LHO ilog, Oct 17 D Sigg).

Chapter 2

Technical noise added to interferometer by squeezing

2.1 Introduction

One reservation about squeezing has been the potential to add technical noise to the interferometer. The lower part of the LIGO detection band (10Hz-10kHz) is crucial for detection of insprials, but also extremely fragile and vulnerable to the environmental noise. While squeezing on a prototype gravitational wave detector and at GEO600 have demonstrated successfully at frequencies above 30kHz and 900Hz respectively, both of these interferometers have orders of magnitude less sensitivity at the crucial region around 100Hz [**?**, **?**]. Past experience has shown that techniques that work well on interferometers at higher frequencies can add unacceptable levels of environmental coupling to a LIGO interferometer. Testing a squeezer on an Enhanced LIGO interferometer gave us the opportunity to demonstrate that squeezing is compatible with good low frequency sensitivity, and to measure the environmental couplings in a regime that is as close as possible to the Advanced LIGO sensitivity. Environmental couplings due to squeezing have caused concern because squeezing involves making modifications to the dark port of the interferometer which is especially sensitive to any noise couplings. However, the possibility of operating the interferometer at normal

sensitivity with the squeezer blocked, or with various parts of the squeezer blocked, allows us to identify and isolate the sources of environmental coupling more easily than in systems without which the interferometer cannot operate with good sensitivity, or systems that are likely to cause lock losses when disturbed.

The results shown in Chapter 3 (check!) clearly show that squeezing did not add noise at any frequencies in the Enhanced LIGO spectrum. Enhanced LIGO was the best possible test bed for Advanced LIGO technologies, and the fact that squeezing was compatible with Enhanced LIGO's sensitivity is the most convincing argument we have that it can be compatible with Advanced LIGO's senstivity. However, Advanced LIGO will be about a factor of ten more sensitive once it reaches design sensitivity, so we have characterized three main sources of technical noise added by the squeezer.

2.2 Noise coupling mechanisms

The mechanism of most concern for Advanced LIGO is backscatter, where light scattered out of the interferometer hits the squeezer and is scattered back into the interferometer creating a spurious interferometer. Any coherent light at the interferometer frequency that enters the OPO, called seeding, is resonantly enhanced and will enter the interferometer along with the squeezed beam and couple acoustic and environmental noise to the interferometer readout. Lastly any amplitude noise on the small amount of coherent locking field that passes through the output mode cleaner could potentially add noise to the detector.

2.2.1 Backscatter

Due to imperfections in the Faraday isolator, a small amount of light from the antisymetric port of the interferometer is sent towards the squeezing table. A second Faraday isolator was installed in the squeezing path to isolate the squeezer from this light, but a small amount of light (3uW) is transmitted through the Faraday towards the squeezer. The optical parametric oscillator used is in a travelling wave configuration so the direct reflection of the

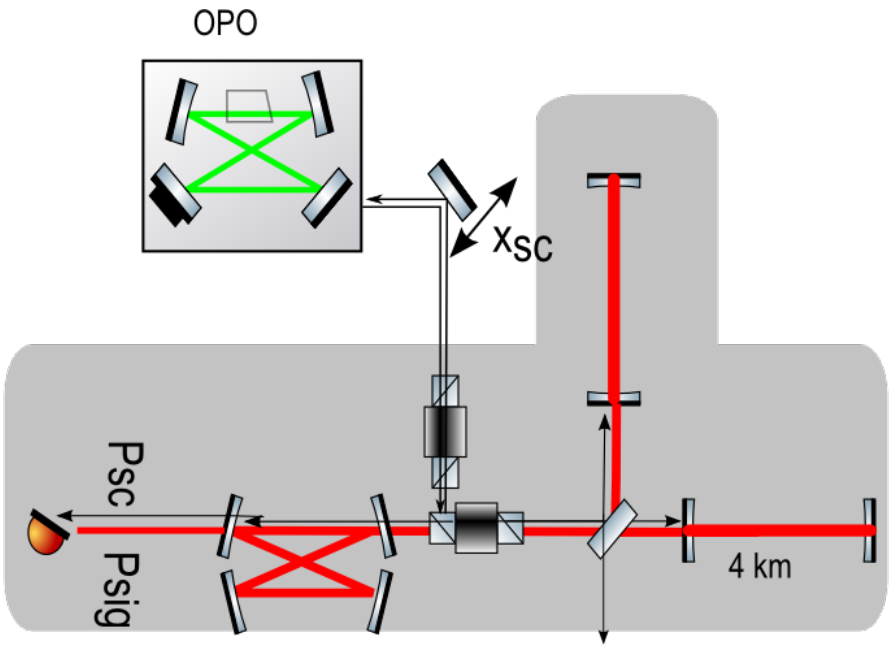

Figure 2-1: Squeezing injected into Enhanced LIGO interferometer. Black arrows represent scattered light, E_{sc} and E_{sig} are the amplitudes of the fields due to scattering and the signal field at the gravitational wave readout photodetector. Path length changes in the scattering path (x_{sc}) will add noise to the interferometer's signal.

scattered light will not return to the interferometer [**?**]. However, imperfections in optics in the squeezing injection path, and especially inside the OPO, causes a small amount of light to be scattered back towards the interferometer and to the gravitational wave readout photodetctor, where it interferes with the signal field and adds noise. The two fields at the photodetectors are $E_{sig}e^{i\phi_{sig}}$ and $E_{sc}e^{i(\phi_{sig}+\phi_{sc})}$, where ϕ_{sc} is the phase due to the scattering path. The intensity at the photodetector (for E_{sc}, E_{sig} both real) is given by

$$\begin{aligned} I_{PD} &= \frac{c}{4\pi}|E_{sig}e^{i\phi_{sig}} + E_{sc}e^{i\phi_{sc}}|^2 \\ &\approx \frac{c}{4\pi}\left(|E_{sig}|^2 + 2E_{sig}E_{sc}\cos\phi_{sc}\right) \end{aligned} \tag{2.1}$$

Where we assume that $E_{sc} \ll E_{sig}$ and ignore higher order terms in E_{sc}. Integrating over the photodetector area the relative intensity noise due to scattering is:

$$RIN_{sc}(t) = 2\sqrt{\frac{P_{sc}}{P_{sig}}}\cos\phi_{sc}(t)$$

The phase of the scattered light ϕ_{sc} changes as the squeezer table and optics move relative to the suspended interferometer $\phi_{sc}(t) = 4\pi\frac{x_{sc}(t)}{\lambda}$. There are two important contributions to $x_{sc}(t)$, a large slowly varying term $\tilde{x}_{sc}(t)$ and a small high frequency component, $\delta x_{sc}(t)$. The slowly varying part is due to the microseism peak in the ground motion, at frequencies between 100-400mHz and often with an amplitude of multiple wavelengths [**?**].

At higher frequencies, in the gravitational wave detection band, the path length changes due to motion of optics on the squeezer table are small compared to the wavelength, and we can use the small angle approximation $kx \ll 1$:

$$\begin{aligned} RIN_{sc}(t) &= 2\sqrt{\frac{P_{sc}}{P_{sig}}}\cos\left(\frac{4\pi(\tilde{x}_{sc}(t) + \delta x_{sc}(t))}{\lambda}\right) \\ &= 2\sqrt{\frac{P_{sc}}{P_{sig}}}\left(\cos 2k\tilde{x}_{sc}(t)\cos 2k\delta x_{sc}(t) - \sin 2k\tilde{x}_{sc}(t)\sin 2k\delta x_{sc}(t)\right) \\ &\simeq 2\sqrt{\frac{P_{sc}}{P_{sig}}}\left(\cos 2k\tilde{x}_{sc}(t) - 2k\delta x_{sc}(t)\sin 2k\tilde{x}_{sc}(t)\right) \end{aligned} \tag{2.2}$$

To get a worst case expression for the noise fluctuating with $\delta x_{sc}(t)$, we can set $\sin 2k\tilde{x}_{sc}(t) = 1$.

$$RIN_{sc}(t) = \frac{8\pi}{\lambda}\sqrt{\frac{P_{sc}}{P_{sig}}}\delta x_{sc}(t) \tag{2.3}$$

$$RIN_{sc}(f) = \frac{8\pi}{\lambda}\sqrt{\frac{P_{sc}}{P_{sig}}}\delta x_{sc}(f) \tag{2.4}$$

We could also use an average over many cycles of $\tilde{x}(t)$ to get an amplitude spectral density:

$$RIN_{sc}(f) = \frac{4\pi}{\lambda}\sqrt{\frac{P_{sc}}{2P_{sig}}}\delta x_{sc}(f) \tag{2.5}$$

When the motion is not small compared to the wavelength, the coupling becomes nonlinear and upconversion of low frequency motion can cause noise in the gravitational wave band. Fringe wrapping occurs when the amplitude of the motion is larger than one wavelength:

$$RIN_{sc}(t) = 2\sqrt{\frac{P_{sc}}{P_{sig}}}\cos\frac{4\pi}{\lambda}\Gamma\cos\omega_l t \tag{2.6}$$

2.2.2 Seeding of the OPO

In addition to light scattered out of the interferometer any other light at the interferometer carrier frequency that originates from the squeezer will also add technical noise to the gravitational wave readout. The main laser on the squeezer table is tuned to the interferometer frequency, and care must be taken in constructing a squeezer to avoid scattering this light into the OPO or towards the interferometer. For this reason the squeezer was built using as many superpolished optics as possible, in a cleanroom to avoid scattering from dust, and multiple dichroic beam splitters were used to remove the field at the fundamental frequency from the second harmonic beam. Any light that does enter the OPO will be on resonance in the cavity, and will either be parametrically amplified or deamplified depending on its phase. Similar to backscattering the relative intensity noise due to seeding is given by:

$$RIN_{sd}(t) = 2\sqrt{\frac{P_{sd}}{P_{sig}}}\cos\phi_{sd}(t)$$

where P_{sd} is the power due to unwanted light and $\phi_{sc}(t)$ is the phase difference of this light from the interferometer signal. The seeding could have multiple paths so the total phase might be complicated, but it will propagate through the OPO and through the squeezing injection path. Since the backscattering noise comes from double passing the injection path

and OPO, one contribution to the phase of the seeded light will be $\frac{\phi_{sc}(t)}{2}$. This means that like backscattered light, the seeded light could cause both a linear coupling and fringe wrapping.

2.2.3 Amplitude noise due to coherent locking field

The squeezing readout (either the gravitational wave readout or the diagnostic homodyne detector) will not be sensitive to phase noise on the coherent locking field becuase of the many megahertz frequency offset from the carrier beam, however, amplitude fluctuations on the coherent locking field will still add noise. The diagnostic homodyne detector must be carefully aligned to have good common mode rejection for both the coherent locking field and the local oscillator, a decription of alignment methods is given in [**?**]. This is especially important for a squeezer which will be used with a gravitational wave detector, where the coherent locking field needs to have enough power to give a good signal to noise for the coherent locking scheme. In the gravitational wave detector, the coherent field is rejected by the output mode cleaner, and only a small fraction of it actually reaches the detector, so the amplitude noise is largerly supressed.

2.3 Technical noise in Enhanced LIGO

2.3.1 Amplitude noise from coherent locking field

Of these three noise mechanisms, the amplitude noise due to te coherent locking field is of least concern. In the gravitational wave detector the output mode cleaner rejects most of the coherent field. For our offset frequency of 29.5MHz and the finesse of 360 in the enhanced LIGO output mode cleaner as we used it, the power transmission for the coherent locking field was 0.016%. 2011 56uW CLF in squeezed beam for 3.2mW incident on OPO

2.3.2 Linear Couplings

Backscatter and seeding, can both linearly couple environmental noise from motion on the squeezer table into the interferometer spectrum. Although the change in path length between the squeezer and the interferometer is often several microns at low frequencies (0.1 to 0.4 Hz), [?] the motion in LIGO's sensitive frequency band is much smaller than one wavelength. No matter which mechanism is responsible, we can use the same techniques to characterize the linear coupling, identify contributions from individual optics, damp their motion and reduce the noise.

By looking at coherences between appropriate environmental monitors and the gravitational wave read out channel (DARM) we can characterize the coupling of noise at the sensor position to the interferometer. In the region around a few hundred Hertz, an accelerometer mounted on the squeezing table revealed coherences from 200-300 Hz, as shown in Figure 2-2. Coherences with environmental sensors can positively identify noise sources, and track reduction of the couling, but there may also be incoherent couplings that add noise to the spectrum.

By increasing the level of motion, and monitoring the noise power spectrum, we can charachterize both incoherent and coherent couplings. By closely watching a spectrum of DARM while bowing individual optics gently enough that neighboring optics were not also moved, we were able to indentify particular fetures in the spectrum with single optics and damp their motion. After damping identified resonances, the spectrum with squeezing injected appears identical to the spectrum with out squeezing, and the noise at specfic frequencies was reduced by at least a factor of ten, as shown in Figure 2-3.

The level of technical noise introduced by the squeezer in the final configuration for the H1 experiment was below the normal level of interferometer noise. In order to estimate the level of noise added, we increased the table motion at a specific frequencies until we added noise was above the normal noise floor, and extrapolate to the level of noise for normal table motion. This technique meassures both coherent and incoherent noise sources when they are small compared to the interferometer noise, but could miss narrow resonances that add

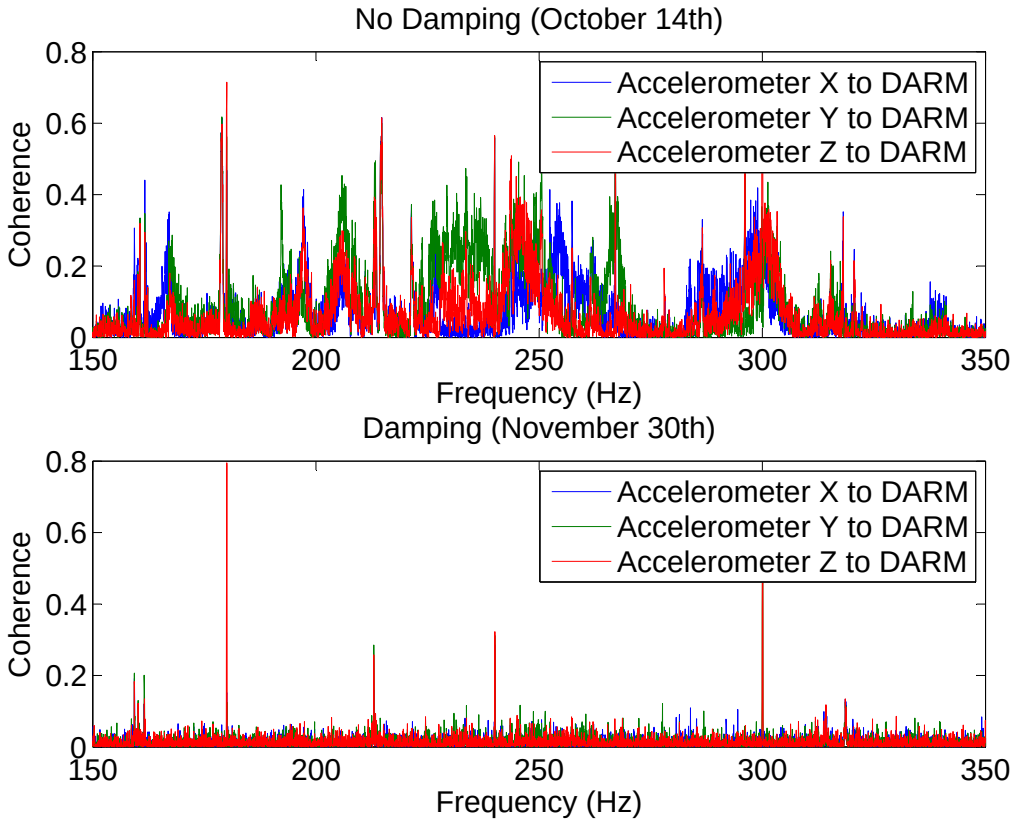

Figure 2-2: Coherence between accelerometers mounted on the squeezer table and the differential arm degree of freedom. The two measurements were made with similar environmental conditions, as measured by the accelerometers. The upper panel shows coherence between 150-300 Hz which was not present when the squeezer was blocked with a black glass beam dump, indicating that the coupling mechanism involved the squeezer [**?**]. Damping the resonances of individual optics identified as responsible for adding noise, as well as other improvements, reduced the coherence with squeezing present as shown in the lower panel.

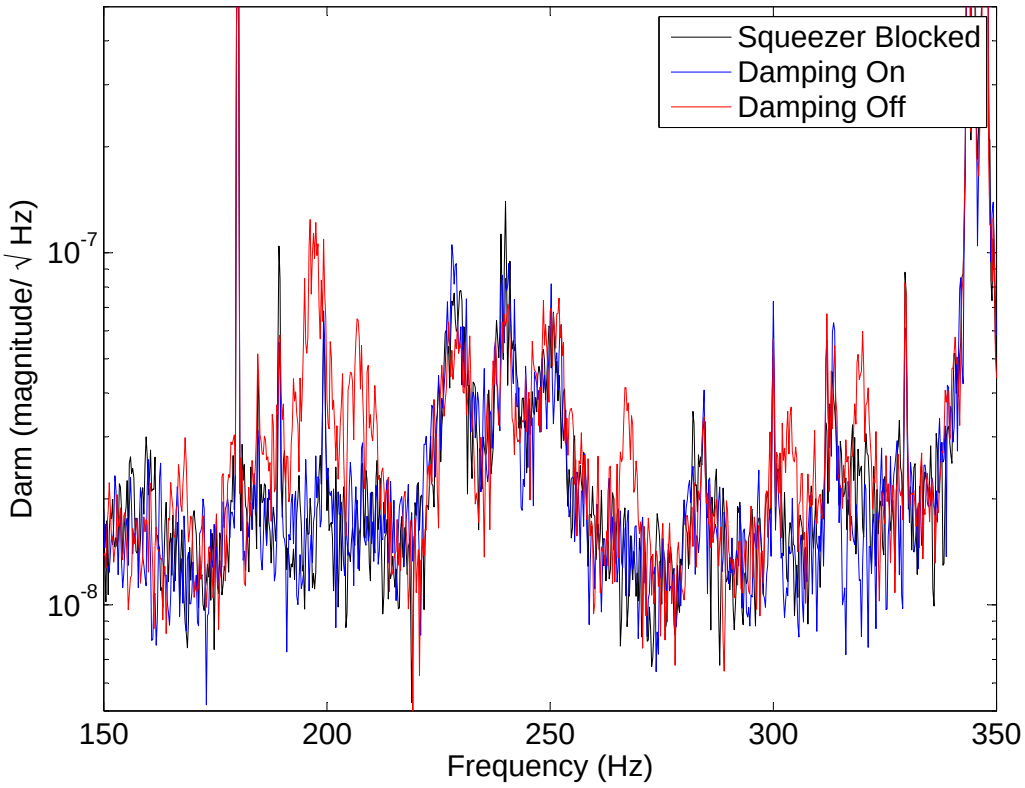

Figure 2-3: Amplitude spectral density of noise in differential arm signal without squeezing injected, and with unoptimized squeezing injected with and without damping material.

higher levels of noise at particular frequencies. Different optic mounts have slightly different resonant frequencies, and all of these optics can contribute to the total motion $\delta x_{sc}(f)$. Using accelerometers we measured the increase in table motion with injections from the shaker, and assumed that the transfer function from the table motion to $\delta x_{sc}(f)$ is linear, although possibly complicated. Assuming only that the accelerometer signal at a particular frequency is proportional to the motion at that frequency we have:

$$\frac{RIN_{off}}{RIN_{on}} = \frac{\delta x_{sc,off}(f)}{\delta x_{sc,on}(f)} = \frac{\delta x_{accel,off}(f)}{\delta x_{accel,on}(f)}$$

Multiple excitation amplitudes at the same frequency were used to confirm that the coupling from table motion to noise on the interferometer output was linear. Spectra were also

recorded with the shaker on and a black glass beam dump on blocking the squeezer port, to check that the squeezer was the dominant mechanism for adding noise from the shaker, rather than electromagnetic couplings or other motion in the corner station, the resulting estimate of the level of noise is shown in Figure 2-4. The measurements made by increasing

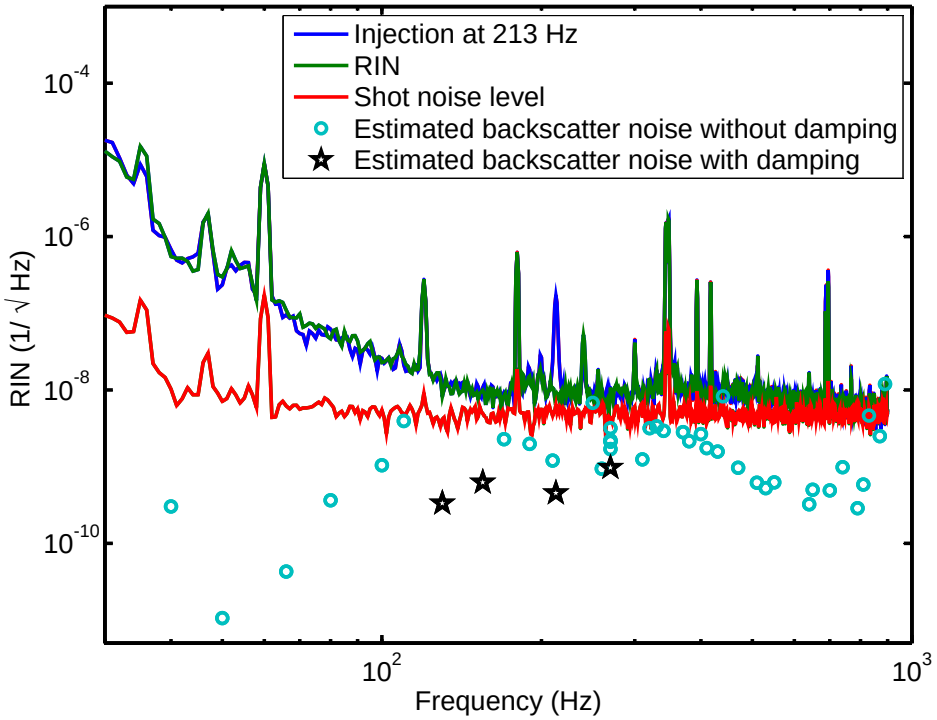

Figure 2-4: Method of estimating level of backscatter noise. The blue and red traces show the relative intensity noise (RIN) at the gravitational wave readout detector under normal conditions and with the squeezer table motion increased at a single frequency. The green trace is the difference photocurrent between the two OMC photo-detectors, which is a measure of shot noise at high frequencies. The light blue circles and black stars are inferred by measuring the noise with injection and comparing table motion as measured by accelerometers with and without an injection.

the motion give us a nice estimate of the total noise, the product of the table motion and

the ratio of scattered power to power in the signal beam.

$$RIN_{sc}(f) = RIN_{off}(f) = RIN_{on} \times \frac{\delta x_{accel,off}(f)}{\delta x_{accel,on}(f)} \tag{2.7}$$

We can use the squeezing angle control signal to infer the change in path length that we nduced by shaking the table, and from that find an estimate of the ratio $\sqrt{\frac{P_{sc}}{P_{sig}}}$. We can also use the accelerometer in the x direction as a measure of the the motion, based on Eq2.5.

$$\sqrt{\frac{P_{sc}}{P_c}} = \frac{\lambda\sqrt{2}}{4\pi} \frac{RIN_{sc}}{\delta x_{sc}(f)} \tag{2.8}$$

The values we get in the final configuration are shown in table **??**

Frequency (Hz)	$RIN_{ifo}/RINsc$	$RIN_{shot}/RINsc$	$\sqrt{\frac{P_{sc}}{P_{sig}}}$ accelerometer	$\sqrt{\frac{P_{sc}}{P_{sig}}}$ error signal
75	143 (lower limit)		NA	NA
130	24.5	12.5	2.24×10^{-7}	0.96×10^{-7}
155	15.9	7.89	2.69×10^{-7}	1.51×10^{-7}
213	14.0	1.97	2.08×10^{-7}	0.49×10^{-7}
270	11.0	4.43	4.91×10^{-7}	0.30×10^{-7}

Table 2.1: Inferred powers at OMC PDs due to seeding at the main laser frequency, before addition of notch.

2.3.3 Distinguishing backscatter from seeding

We would like to distinguish between carrier light that seeds the OPO by backscattering from the interferometer and light that comes from another path on the squeezing table. One effective method to do this is to introduce a frequency offset between the squeezer main laser and the interferometer carrier and lock every control loop other than the final squeezing angle control loop. Using this technique, we were able to identify and eliminate our on table seeding. The ratio of the rms area of the lump around 2 kHz, with the background due to anti squeezing subtracted in quadrature, to the average DC photocurrent is proportional to

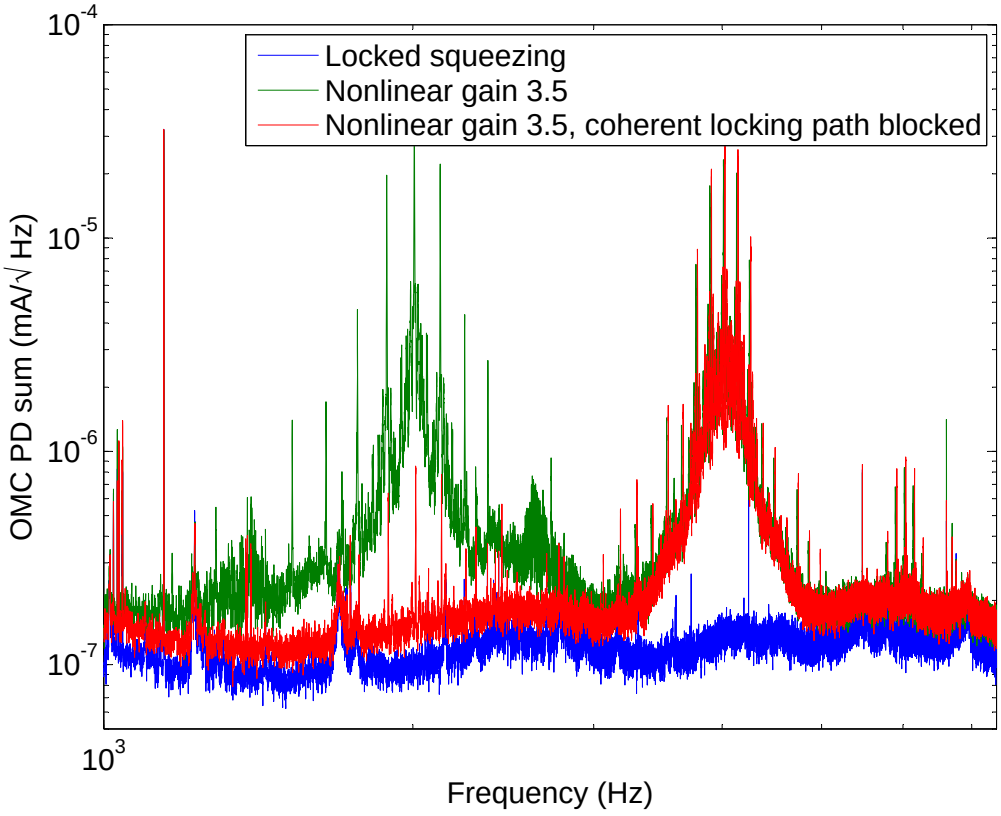

Figure 2-5: Method of distinguishing backscatter from other seeding paths. The blue trace is a reference spectrum with squeezing injected and the squeezing angle controled, while the other traces have a 2 kHz offset between the interferometer carrier frequency and the squeezing main laser. Since the squeezing angle is rotating at 2kHz, the added antisqueezing raises the noise floor at all frequencies. The beat between the interferometer carrier and light at the squeezer main laser frequency is shifted up to 2kHz, while some of the light scattered into the OPO from the interferometer is unconverted by the nonlinear process to kHz. By blocking various paths on the table, and locking and unlocking various loops, we were able to identify the source of seeding on the squeezer table, illustrated by the red trace where the seeding is gone when the coherent field path is blocked.

$\sqrt{\frac{P_{sd}}{2P_{sig}}}$. This measurement was done for three different nonlinear gains, and the results are shown in table 2.4 The source of our seeding was RF pickup at the offset frequency on the cable driving the EOM in the auxiallary laser path, which added a sideband to the auxillary laser at the main laser frequency. The -80 dBm of pickup does not seem to explain the level of seeding we saw, predicting 9.7376e-017 Watts out of the OPO with no nonlinear

Nonlinear gain	$\sqrt{\frac{P_{sd}}{P_{sig}}}$	P_{sd}
1.1	5.2×10^{-6}	0.64nW
3.5	4.2×10^{-6}	0.41 nW
9.47	1.1×10^{-5}	2.7nW

Table 2.2: Inferred powers at OMC PDs due to seeding at the main laser frequency, before addition of notch.

gain. Nonetheless, notching out the pick up eliminated our seeding, so that with the notch installed the spectrum showed no peak at the main laser offset frequency. We saw that this also eliminated excess noise in the interferometer spectrum that was proportional to the power used in the coherent field.

Nonlinear gain	$\sqrt{\frac{P_{sd}}{P_{sig}}}$	P_{sd}
3.5	5.2×10^{-6}	0.64nW
3.5	4.2×10^{-6}	0.41 nW
9.47	1.1×10^{-5}	2.7nW

Table 2.3: Inferred powers at OMC PDs due to seeding at the main laser frequency, before addition of notch.

We can similarly measure the power in the downconverted backscattered light.

2.3.4 Measuring power at the detector due to backscatter

Fringe wrapping provides a more direct way to measure the total backscattered power. We used a longitudinal piezo electric in the injection path to modulate the path length my many wavelengths while keeping the squeezing angle locked. While the backscattered light double passes the modulated mirror, the on table seeding is only modulated once. This means we are adding noise in the time domain due to both backscattered light and seeding from the squeezer table:

$$RIN(t) = 2\sqrt{\frac{P_{sc}}{P_{sig}}}\cos\left(\frac{4\pi\Gamma}{\lambda}\cos\omega_l t\right) + 2\sqrt{\frac{P_{sd}}{P_{sig}}}\cos\left(\frac{2\pi\Gamma}{\lambda}\cos\omega_l t\right)$$

As shown in Figure 2-6 in the frequency domain this will produce a distinct shelf in the spectrum, which we can fit to find the amount of backscattered power. With this mea-

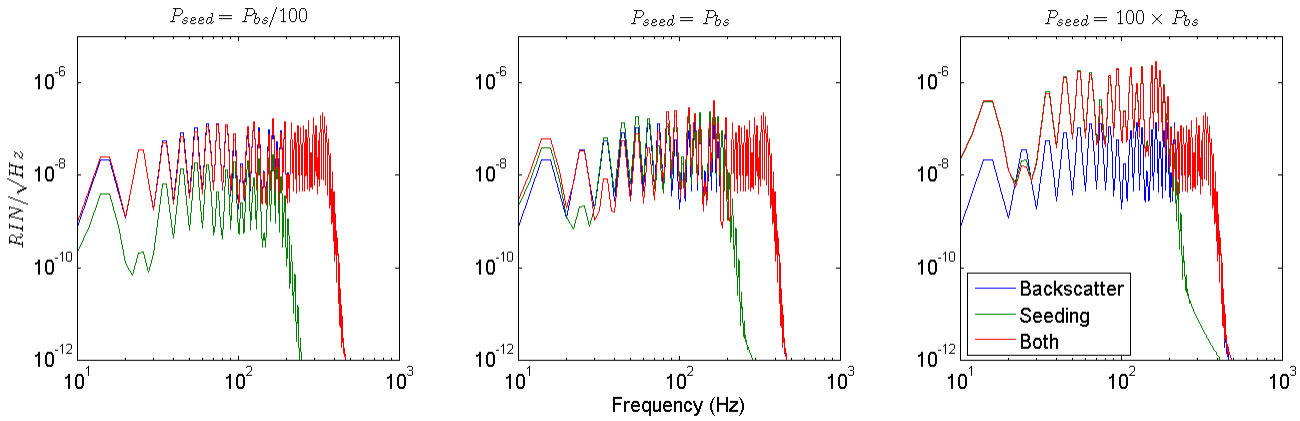

Figure 2-6: In the frequency domain, the fringe wrapping feature is dominated by backscattered light, unless the power due to direct seeding from the squeezer table is much larger.

surement done in the final configuration, (shown in Figure 2-7) we find that the power due to backscatter at the output mode cleaner photodetectors is $0.62 \pm 0.04nW$, and the ratio $\sqrt{\frac{P_{sc}}{P_{sig}}}$ is $7.25 \times 10^{-6} \pm 0.25 \times 10^{-6}$. This measurement was taken with a nonlinear gain of 6.2, and with the squeezing angle approximately tuned to squeezing. Because the cavity is nonlinear, the amount of amplification of backscattered light in the OPO depends on both the nonlinear gain and the squeezing angle.

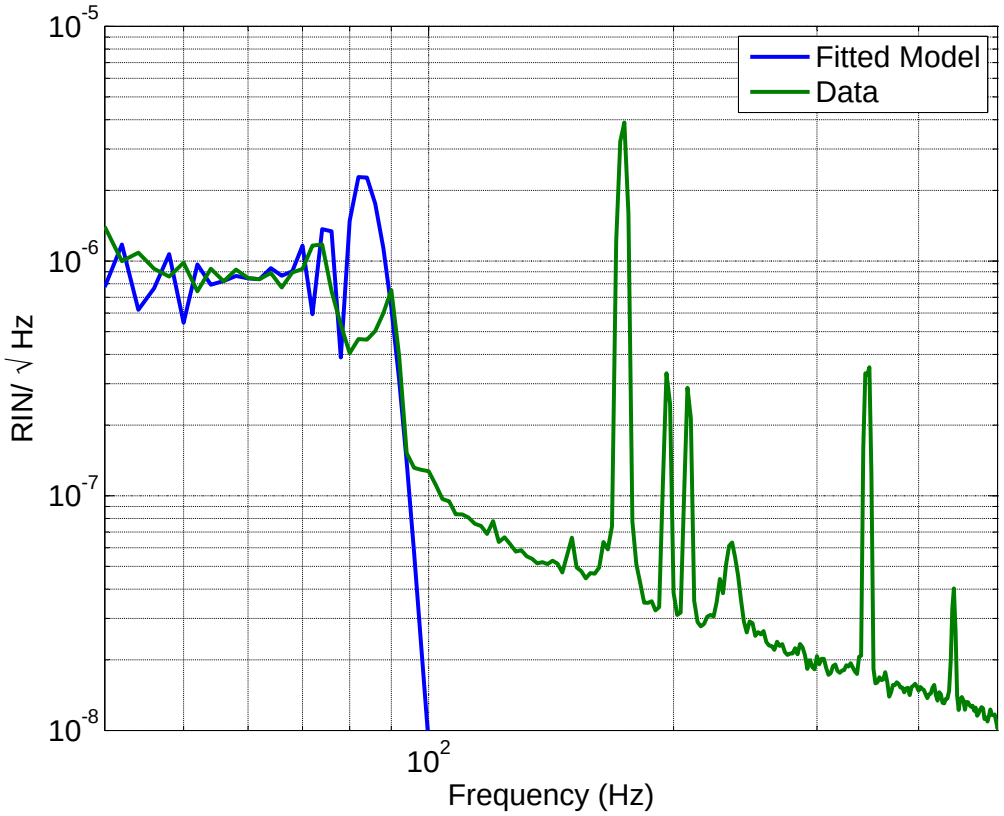

Figure 2-7: Fringe wrapping result with squeezing in final configuration. The blue trace is a fit to the part of the spectrum which is dominated by fringe wrapping only. The red trace is the relative intensity noise measured while the injection path length was modulated by many wavelengths and the squeezing angle kept locked. The suppression of the differential arm control loop is removed from the red trace.

2.4 Requirements for Advanced LIGO

We would like the noise introduced by backscatter from the squeezer to be a factor of ten below the interferometer sensitivity at all frequencies. Since Advanced LIGO will be limited by shot noise down to (?)Hz, we can compare the high frequency relative intensity noise due to scatter to the relative intensity noise due to the squeezed shot noise. The amplitude spectral density of RIN due to shot noise will be:

$$RIN_{shot} = \frac{1}{2}\sqrt{\frac{2hc}{\eta P_{sig}\lambda}} \tag{2.9}$$

where the factor of 1/2 is due to the 6dB of squeezing we hope to implement, and η is the photo-detector quantum efficiency. We can now place a requirement on the backscattering noise:

$$\frac{RIN_{sc}}{RIN_{shot}} = 4\pi\sqrt{\frac{\eta P_{sc}}{\lambda hc}}\delta x_{sc}(f) \leq \frac{1}{10} \tag{2.10}$$

Our measurements with the shaker injection showed that factor between 0.16 and 1, so we would like to improve by about a factor of 10.

2.4.1 Factors that influence $\sqrt{\frac{P_{sc}}{P_{sig}}}$

$$P_{sc} = P_{as}\left|\frac{P_{carr}}{P_{tot}}\right|_{as} R_{OF}T_{SF}M_{OPO}R_{OPO}\frac{1}{2}\eta_{det} \tag{2.11}$$

The backscattered power depends on several factors, and is proprtional to the power headed from the interferometer towards the antisymetric port, P_{as}. We are only concerned about power at the carrier frequency, so we only consider the fraction of the power at the antisymetric port that is at the carrier frequency. The next four terms are illustrated in Figure 2-8, and tell us the amount of power incident towards the AS that will be sent back towards

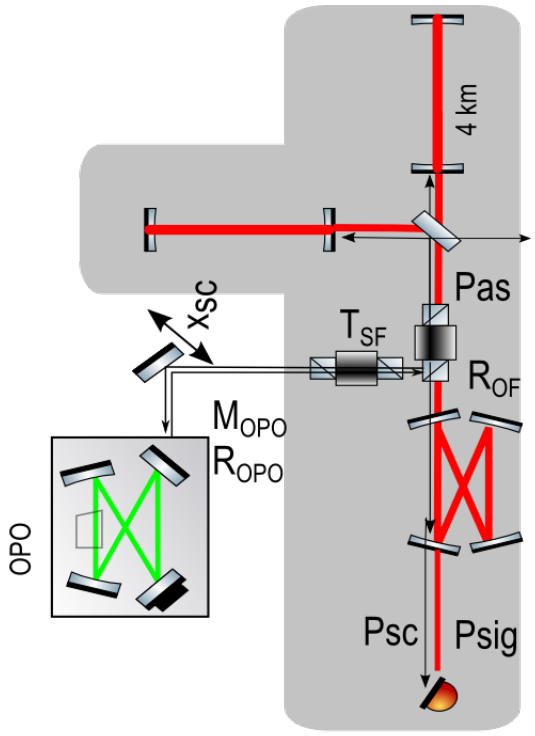

Figure 2-8: Factors that contribute to amount of scattered power: P_{as} is the amount of power heading towards the antisymetric port from the interferometer, R_{OF} is the power reflectivity of the output faraday towards the squeezing injection path, T_{SF} is the transmission in reverse of the squeezing injection faraday, M_{OPO} is the amount of power from the amount of power in the AS beam that is in the right polarization and spatial mode to enter the OPO, R_{OPO} is the fraction of the power that enters the OPO that will be scattered into the direction propagating towards the interferomter.

the interferomter after scattering off of the OPO. Light entering at the antisymetric port will either scatter into the common or the differential mode, we will assume that half the power enters each mode since the microseism can move the squeezing table by a full fringe. The detection efficiency η_{det} for squeezing tells us how much of the power in the OPO mode reaches the antisymetric port, to acheive 6 dB in advanced LIGO we would like this to be 80%.

Our measurements of some of these parameters are:

Parameter	Shaker Test	Advanced LIGO prediction
P_{as}	$300mW$	-
$\left\|\frac{P_{carr}}{P_{tot}}\right\|_{as}$	$\frac{1}{5}$ [**?**]	-
P_{sig}	$10.96mW$	-
R_{OF}	0.5% [**?**] measured in lab	same
T_{SF}	0.02% [**?**] measured in lab	same
$R_{OF}T_{SF}$	0.001% installed	lab performance
M_{OPO}	1/3- 1/100 (?) [**?**]	
η_{det}	38%	80%

Table 2.4: Factors that contribute to P_{sc}.

The most uncertain of these parameters is M_{OPO} the fraction of the scattered power incident on OPO that is in the right mode to couple into the OPO. We know that almost all of the scattered light was in the correct polarizaition, measured by placing a polarizing beam splitter in the beam. We also placed a photodetector to monitor the scattered light reflection off of the OPO input coupler and monitored the reflected power as we scanned the OPO. This shows us that no single spatial mode dominates, and can give us an upper limit on the mode matching. However, we weren't able to positively identify any of these peaks with the mode that will resonante inside the locked OPO, and so we cannot get a direct estimate of the mode matching. If we assume that 1/10th of the power is mode matched into the OPO, we find that R_{OPO} is -43dB.

The signal power on the output mode cleaner photodiodes, P_{sig}, is also related to P_{as}:

$$P_{sc} = P_{as}\left|\frac{P_{carr}}{P_{tot}}\right|_{as} M_{OMC}T_{OMC}$$

where M_{OMC} is again the fraction of the power incident on the output modecleaner from the antisymetric port that is in the right spatial and polarization mode to resonante in the OMC, and T_{OMC} is the transmission of the carrier 00 mode through the OMC. Combing the two expressions gives a ratio:

$$\frac{P_{sc}}{P_{sig}} = R_{OF} T_{SF} \frac{M_{OPO}}{M_{OMC}} R_{OPO} \frac{\eta_{det}}{2T_{OMC}}$$